

# The EXODET Apparatus And Its First Experimental Results: $^{17}\text{F}$ Scattering By $^{208}\text{Pb}$ Below The Coulomb Barrier

M. Romoli<sup>1</sup>, M. Mazzocco<sup>3</sup>, R. Bonetti<sup>5</sup>, A. De Francesco<sup>1</sup>,  
A. De Rosa<sup>1,2</sup>, M. Di Pietro<sup>1</sup>, T. Glodariu<sup>3,9</sup>, A. Guglielmetti<sup>5</sup>,  
G. Inghima<sup>1,2</sup>, M. La Commara<sup>1,2</sup>, B. Martin<sup>1,2</sup>, V. Masone<sup>1</sup>,  
P. Parascandolo<sup>1</sup>, D. Pierroutsakou<sup>1</sup>, M. Sandoli<sup>1,2</sup>, P. Scopel<sup>3</sup>,  
C. Signorini<sup>3</sup>, F. Soramel<sup>4</sup>, L. Stroe<sup>6</sup>, E. Vardaci<sup>1,2</sup>, J. Greene<sup>7</sup>,  
A. Heinz<sup>7</sup>, D. Henderson<sup>7</sup>, C. L. Jiang<sup>7</sup>, E. F. Moore<sup>7</sup>, R. C. Pardo<sup>7</sup>,  
K. E. Rehm<sup>7</sup>, A. Wuosmaa<sup>7</sup>, J. F. Liang<sup>8</sup>

<sup>1</sup> INFN, Sezione di Napoli, Via Cintia, I-80125, Napoli, Italy.

<sup>2</sup> Università degli studi di Napoli "Federico II", Dip. Sc. Fis., Via Cintia, I-80125, Napoli, Italy.

<sup>3</sup> Università di Padova and INFN, Sezione di Padova,..... Italy .

<sup>4</sup> Università di Udine and INFN, Sezione di Udine,..... Italy.

<sup>5</sup> Università di Milano and INFN, Sezione di Milano,..... Italy.

<sup>6</sup> INFN, Laboratori Nazionali di Legnaro,..... Italy .

<sup>7</sup> ANL, Argonne, Illinois, .....USA .

<sup>8</sup> ORNL, Oak Ridge, Tennessee,..... USA .

<sup>9</sup> Glodariu institution.....

**Abstract.** A new detector apparatus has been appositely designed and developed to be used in experiments performed with radioactive ion beams. It consists of 16 highly segmented silicon strip detectors arranged in two-layer telescopes and subtending a large total solid angle (about 70% of  $4\pi$  sr). An innovative read-out system for the position information, that uses highly integrated electronics (ASIC chips), has been implemented. The energy information read-out has been obtained using standard nuclear electronic chains. A first successful experiment has been performed at the Argonne National Laboratory (USA), studying the  $^{17}\text{F}$  scattering by a  $^{208}\text{Pb}$  target, at 90.4 MeV of incident energy. The  $^{17}\text{F}$  angular distribution has been analyzed and the optical model potential best-fit parameters determined. The same analysis performed on  $^{17}\text{F}$  data taken at higher incident energy, in completely different experimental conditions, gives consistent results, and the comparison with analogous experiments performed with stable beams ( $^{19}\text{F}$ ,  $^{16}\text{O}$ ,  $^{17}\text{O}$ ) indicates a behavior for the  $^{17}\text{F}$  more similar to that of the Oxygen isotopes than to the  $^{19}\text{F}$  one. Despite the short data collection time, also the cross section for the  $^{17}\text{F} \rightarrow ^{16}\text{O} + p$  break-up process has been evaluated.

## INTRODUCTION

The study of radioactive and exotic nuclei is a useful tool to get information about the behavior of the nuclear potential when the interaction radius, due to the external loosely bound nucleons, can be very different from that of the stable nuclei in the same mass region. In these extreme conditions of the nuclear matter, the effect of such a spatially extended nuclear density (nuclear halo or skin) on the reaction mechanism cross sections is not clearly understood. The possibility to evidence the presence of new typical features for such nuclei seems to increase around the Coulomb barrier energy region, where several interesting mechanisms are in competition (elastic and inelastic scattering, break-up and stripping break-up, complete and incomplete fusion).

The interest for the experimentation with radioactive ion beams (RIBs) is growing up at the moment, but practical limitations rise up from the very low beam intensities ( $10^5$ - $10^6$  pps) presently available at the first generation RIB accelerator facilities. To partially overcome such limitations, the project of a new RIB measurement requires the utilization of a charged particle detector system subtending a solid angle as large as possible. Moreover high energy resolution and position sensitivity, that means high granularity of the system, are also required in order to reconstruct the ejectile momentum distribution.

In this framework, we have developed a new experimental apparatus for charged particle detection and identification, named **EXODET** (an acronym for **EXOTIC DETECTOR**) and appositely designed to be used in RIB experiments. In the next section, the main features of such apparatus will be described. Due to the high segmentation of the detector array (counting 1600 elements), it has been necessary to use a non-standard highly integrated read-out system for the position information (ASIC chips), while for the energy information treatment we used standard nuclear electronic chains. In the following, a section has been dedicated to the read-out electronics description.

The EXODET apparatus has been successfully used, for the first time, at the Argonne National Laboratory (USA), to study the scattering of the exotic  $^{17}\text{F}$  beam by  $^{208}\text{Pb}$  at an incident energy just below the Coulomb barrier. The experimental layout of the performed measurement, the analysis of the data collected and the comparison of the obtained results with theory and different nuclei data analyses will be the arguments of the last two sections, together with final comments and considerations.

## THE EXODET APPARATUS

The basic EXODET apparatus module consists of a large active area silicon detector, produced and delivered by MICRON Semiconductors Ltd, following a Naples custom design. The detector active area is  $50 \times 50 \text{ mm}^2$  large and the total occupancy of the die is  $53 \times 53 \text{ mm}^2$ , due to the guard rings and the passivated region surrounding the active area. A G-10 support is placed under such  $1.5 \text{ mm}$  wide unusable region to ensure a safer handling of the die and the transparent transmission through the detector stack with the minimum dead zone.

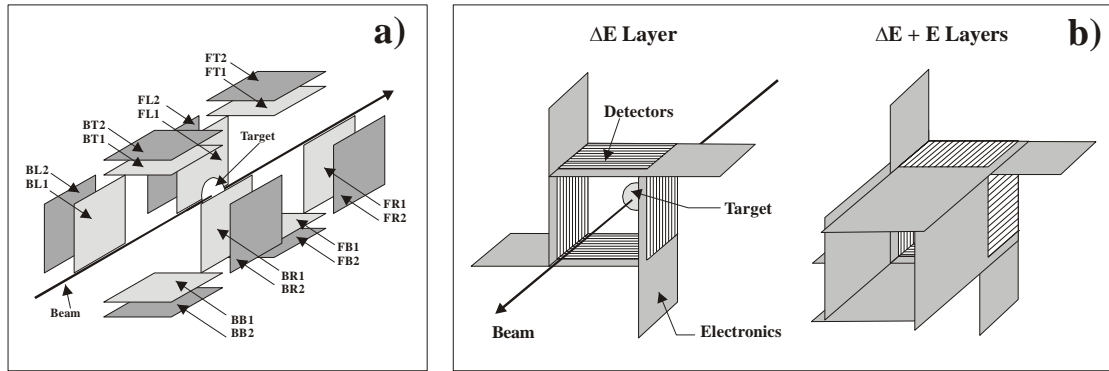


**FIGURE 1.** a) Layout of the EXODET detectors. b) Assembling of the EXODET detectors. Note the direction of the strips of the  $\Delta E$  and E layers with respect to the beam one.

The detector front side active area is segmented in 100 strips, having a pitch size of 0.5 mm and a separation distance of 50  $\mu\text{m}$ . Each strip is wire bonded to an external golden copper pin. The ohmic rear side of the detector is not segmented and is used to get the particle energy loss signals. Detectors with different thickness are available (40, 60, 100  $\mu\text{m}$  for the  $\Delta E$  layer and 150, 500, 1000  $\mu\text{m}$  for the E layer), but in the standard configuration 60  $\mu\text{m}$  and 500  $\mu\text{m}$  thick detectors are mounted as  $\Delta E$  and E detectors, respectively.

16 of such detectors are arranged in 8 two-layer telescopes, allowing the identification in atomic number of the particle passing through the first layer by means of the usual  $\Delta E$ -E technique. In fig.1a) is shown the displacement of the telescopes around the target in the forward and backward hemispheres with respect to the beam direction and the target position. The identification code used for the detectors consists of three characters XYN, where X=F (Forward) or B (Backward), Y=T (Top) or B (Bottom) or R (Right) or L (Left), N=1 ( $\Delta E$  detector) or 2 (E detector). The strips of the  $\Delta E$  layer are placed perpendicularly to the beam direction, while the E detector strips are in the same direction of the beam, as shown in fig.1b). In such a way, it is possible to determine the position of a particle passing through the first layer and reaching the second one with an indetermination of  $0.5 \times 0.5 \text{ mm}^2$ . The detection pixels so defined subtend different solid angles and  $\theta$  scattering angle ranges depending on their position and distance from the target. We used Monte-Carlo calculations to evaluate the geometrical efficiency for each part of the EXODET apparatus. Also for the particles stopping in the first layer, the  $\Delta E$  strip displacement and the utilization of such Monte-Carlo codes allow to extract information about the particle angular distribution, although with a higher indetermination, due to the non-spherical shape of the EXODET detectors. The total solid angle subtended by the whole EXODET apparatus is about 70% of  $4\pi \text{ sr}$ .

In fig.2a) is shown a photo of two EXODET detectors before their assembling to form a single telescope. The detectors are already glued and connected to the PCBs containing the detector-chip interface electronics and the preamplifier used for the energy signal treatment. A photo of the whole EXODET apparatus mechanics is shown in fig.2b). The reduced size of the apparatus, 350 mm in the beam direction and

230 mm in the other two, without cabling, and its compactness allow an easy transportation to different laboratories and the possibility to be used, as ancillary charged particle detector, in more complex experimental set-up.

A cooling system, that uses Peltier cells and water as cooling fluid, ensures the appropriate detector temperature control and stabilization.

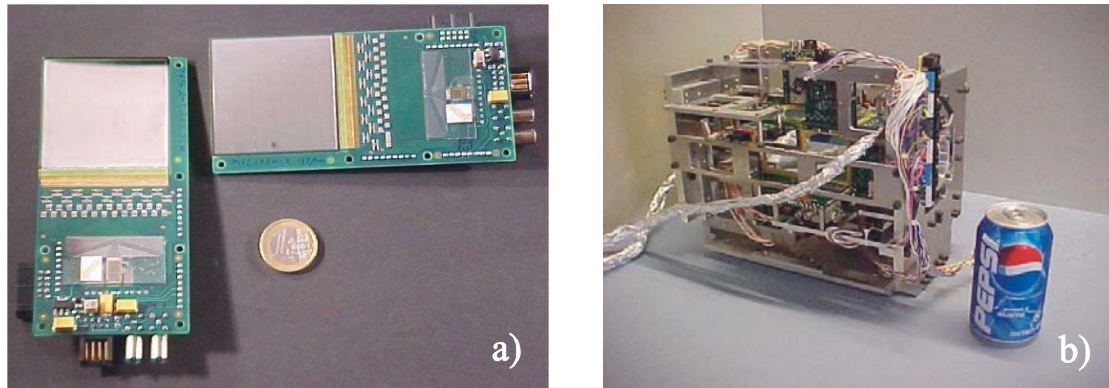


**FIGURE 2.** a) The two detectors of one EXODET telescope before their assembling. The 1 Euro coin is shown for size comparison. b) The whole EXODET apparatus mounted on its own mechanical support. The comparison with the can size gives an idea of the EXODET compactness.

## THE ELECTRONIC READOUT

The information about the energy released into the EXODET apparatus by the impinging particles is obtained from the rear side of each detector that is not segmented. The energy signal treatment is carried on using a standard nuclear electronic chain, consisting of a low noise preamplifier, a spectroscopy amplifier and an ADC for the signal amplitude analysis. The timing output of the amplifier is sent to a CFD in order to obtain a logic signal, used for the trigger analysis and generation (see fig.4a)). The most interesting part of this typical electronic chain is the new low-cost hybrid charge preamplifier, named CHAPLIN (CHARGE Preamplifier Low-noise INFN Napoli), which has been completely designed and developed by the Electronic Service of the INFN – Sezione di Napoli. The main features of such device are: 1) a sensitivity of 28 mV/MeV (or 5 mV/MeV); 2) a noise at  $C_{\text{source}}=0$  pF of 300 e rms; 3) a Risetime at  $C_{\text{source}}=2$  pF of 22 ns; 4) a Falltime at  $C_{\text{source}}=2$  pF of 3.3  $\mu$ s; 5) a power dissipation of 180 mW. This preamplifier has been already successfully used for several different experimental apparatus.

For the positional information readout we could not use standard electronic chains, being the cost prohibitive because of the elevate number of channels to be analyzed (1600 for the whole apparatus). So we developed a new readout system based on highly integrated electronic circuitry, namely an ASIC chip. This chip, originally developed for high-energy particle physics experiments [1], has been found suitable also for our purposes, with an opportune design of the detector-chip interface. In particular, we implemented a resistive attenuator, with an attenuation factor of 70, to match the strip signals into the dynamic range of the chip and we designed a pitch adapter to reduce the pitch size from 0.5 mm at the detector end to about 80  $\mu$ m at the

chip end. On the detector-chip interface board are also located the connectors for the communication lines of the chip I/O, for the energy signal output, and for the power supplies of chip, preamplifier and detector.

Each chip, having a size of  $5.7 \times 8.3 \text{ mm}^2$ , drives up to 128 input channels, so we used one chip for each detector, connecting the strips of the detector to the first 100 lines. Inside the chip, both the analogical and the digital treatments of the signals, coming from each strip, are performed contemporarily and separately. In fig. 3 is shown a scheme of the single channel electronics contained into the chip. The input signals are pre-amplified and shaped, then a sampling of the input line voltage is performed at a frequency of 15 MHz and compared to the threshold voltage  $V_{\text{THRESH}}$ , externally settable via a 6-bit DAC, with a 7.5 mV step. When the input signal is higher than  $V_{\text{THRESH}}$ , a bit of the cyclic memory buffer is set to 1. If an external trigger command arrives to the chip, this sampling procedure is stopped and the digital circuitry of the chip analyzes the memory buffer to find a bit to 1, when it happens, the chip gives in output an already digitalized information stream containing the event identification header, the identification number of the hit strips and, for each of them, the ToT (Time over Threshold) and the JT (Jitter Time). The ToT is the time spent by the input signal over the threshold, measured in clock hit number, with a sensitivity of 67 ns, while the JT is the time distance, expressed in clock hit number, between the input signal and the trigger arrivals. The ToT is roughly proportional to the energy lost into the detector and the JT is a sort of correlation time useful to disentangle spurious events to the trigger correlated ones, as shown in the following section. In the used set-up, the chip conversion gain was 150 mV/fC, the signal memory buffer length was 12  $\mu\text{s}$  (193 cells) and the signal analysis window was 2  $\mu\text{s}$  (32 cells).

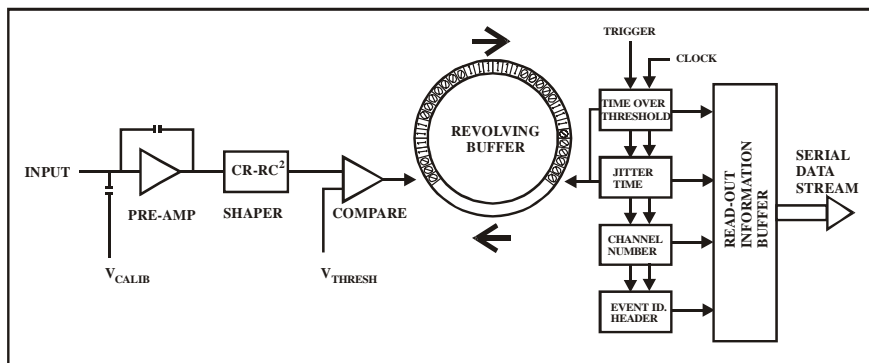


**FIGURE 3.** Simplified electronic scheme of the ASIC chip used for the positional information readout of the EXODET apparatus.

In fig.4a), is reported the scheme of the electronic chain used for one of the EXODET detectors. We have developed several new front-end electronic boards, interfaced to the VME bus, and a new data acquisition system, named **VIPER** (**V**ME Interfaced to **P**CI **E**XODET **R**eadout), has been designed from scratch to manage the readout from homemade and commercial electronic modules. We decided to base the new developments on the VME bus because of its widespread use in nuclear physics laboratories and for the large variety of front-end modules (ADC, TDC, QDC, scalers...) commercially available. The dark colored boxes in fig.4a) represent the new

components hardware and software appositely developed. The interface between the ASIC chips and the VME bus is ensured by the AVI boards (ASIC to VME Interface), one card for each chip. The TS board (Trigger Supervisor) is a highly versatile board and is the trigger filter and deliverer for the whole front-end. The AVI board manages the communication channels between the chip and the VME bus for operations like sending setup or calibration commands to the chip. When the acquisition is running and the TS board asserts a valid trigger signal, the AVI sends the trigger command to the chip and makes available to the VME bus the data stream received from the chip. Signals regarding the internal status of the AVI board and/or the chip connected to it are sent, via the control bus, back to the TS board which, in turn, has also the role of reporting occurrences of errors, FIFO half-full signals, and other important control signals.

Another important task performed by the TS board is the logical combination (OR/AND) of all the input channels deputed to provide a trigger signal. When a channel proposes a trigger signal, before promoting it to a valid trigger, the TS board controls that the whole system is ready (i.e., no AVI is busy, no error occurred, acquisition is running,...). It is possible to mask or sample one or more of the input channels and to force a valid trigger assertion for testing purposes. An external inhibit signal can also be used to integrate commercial boards in the readout system. This is the case for the ADC used to encode the energy signal from the silicon detector: the inhibit signal comes from the ADC, and is kept asserted by the ADC itself until the data digitization cycle has been completed. To evaluate the dead time, the TS board has been equipped with rate meters and counters for the proposed and accepted triggers. Furthermore, dividers by 10/100/1000 can also be used for the input channels. Finally, the TS board is also used to synchronize all the front-end boards in order to guarantee a common time stamp.

To ensure a complete reconfiguration of the developed electronics and flexibility with respect to wider experimental requirements, FPGAs have been extensively used in the design of the boards along with advanced techniques to optimize the connection arrangement between them. Also the AVI and TS boards have been developed by the Electronic Service of the INFN – Sezione di Napoli.

The VME bus is connected to a PC via a commercial VME-PCI bridge. This solution reduces the problems due to the CPU obsolescence, allows a progressive low-cost enhancement of the DAQ system performances with the upgrade of the CPUs available on the market, and does not link the DAQ software to a specific platform. The choice of transferring the CPU from the VME bus to the PC also allows taking the most advantage from the continuous improvement of the I/O devices (disks, RAM, DVD writer...) of the PC industry. One of the VIPER DAQ software components has been designed on the basis of a *Producer/Consumer* model: the *Producer* is the readout process and the *Consumers* are processes like event buffering, delivering, storing, and histogramming. Both the architecture and the hierarchy of the processes are suitable for a multiprocessor environment built on a multinode configuration. The whole system, schematically shown in fig.4b), is accessible over the network because of a *Server/Client* architecture. The *Server* is the process that manages the hardware and runs on the PC directly linked to the front-end. The *Clients* operate on the front-end and monitor the data acquisition through the *Server*. The DAQ system can manage

more than one VME crate and includes an innovative and general method to setup the front-end modules, and the relative on-line analysis, which eliminates the burden due to the implementation of software drivers for new modules. The user can quickly operate a new module without the need of intervention on the DAQ core software. The whole software has been developed in the C/C++ languages for the Linux operating system platform, and using the OSF/Motif environment for the graphical user interface.

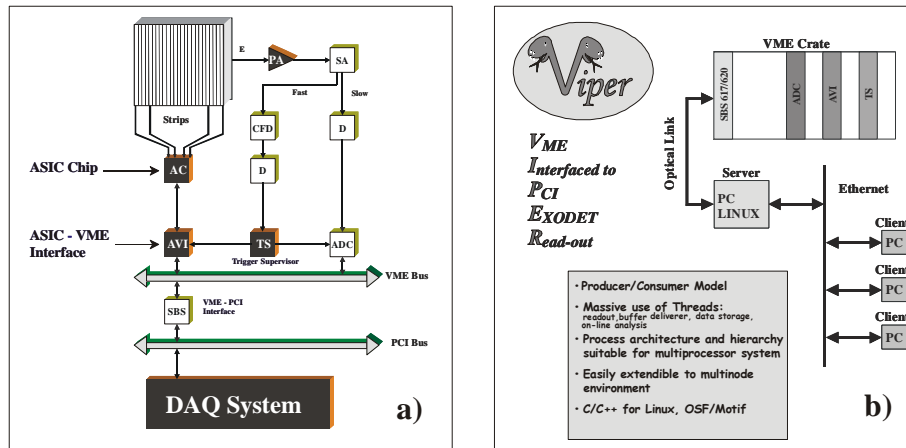


**FIGURE 4.** a) Scheme of the electronic chain for one of the EXODET detectors. The dark colored boxes represent homemade electronics or software, whereas the white ones represent commercial equipments. b) Schematic drawing of VIPER. The front-end VME crate is linked to a personal computer via a VME-PCI bridge board. The DAQ software runs on a Linux environment and the whole system is accessible over the network.

## THE $^{17}\text{F}$ SCATTERING EXPERIMENT

The first experiment performed using the EXODET apparatus has been the study of the  $^{17}\text{F}$  scattering by a  $^{208}\text{Pb}$  target at 90.4 MeV of incident energy. The  $^{17}\text{F}$  beam was produced as secondary beam at the RIB facility of the Argonne National Laboratory (USA), using the inverse kinematics reaction  $p(^{17}\text{O}, ^{17}\text{F})n$ , with an average intensity of about  $10^6$  pps. The target was a self-supporting  $1 \text{ mg/cm}^2$  thick  $^{208}\text{Pb}$  foil. The main beam contamination came from the  $^{17}\text{O}$ , having the same magnetic rigidity but with an energy about 64/81 times the  $^{17}\text{F}$  one. At these energies both the  $^{17}\text{O}$  and  $^{17}\text{F}$  scattered ions are completely stopped into the  $\Delta E$  layer of the telescopes. For this experiment only a section of the whole EXODET apparatus, consisting of two telescopes, was used. From the telescope placed in the backward hemisphere, subtending the scattering angular range  $\theta_{\text{lab}}=98^\circ\text{-}154^\circ$ , both the position and energy information were taken. The detector placed in the forward hemisphere ( $\theta_{\text{lab}}=26^\circ\text{-}82^\circ$ ) was used for normalization purpose, being the scattering purely Rutherford at the angle and energy ranges here considered, and we readout from it only the energy information. The trigger for the data acquisition system was obtained by the OR of all the energy signals. In the upper panel of fig.5a) is reported the energy spectrum of the  $\Delta E$  backward detector. The two bumps in the high energy side correspond to the  $^{17}\text{F}$  (at the higher energy) and  $^{17}\text{O}$

scattered ions. Their broadening is mainly due to the kinematics spread of the particle hitting the detector, which subtends a solid angle of about 110 msr, and to the energy lost in the target. The overall energy resolution was evaluated to be about 6-8%. A better resolution can be achieved selecting a limited number of strips at the cost of a lower statistics. On the left side of the spectrum a peak is visible at around 8 MeV mainly originated from light particles. Gating the  $\Delta E$  spectrum with conditions on the information obtained from the strips, it is possible to select the contributions coming from  $^{17}\text{F}$  ions and from the light particles, as shown in the middle and lower panel of fig.5a), respectively. In the upper panel of fig.5b) is reported the JT spectrum of the  $\Delta E$  backward detector, showing a sharp peak for JT=10, which evidences the time correlation of the collected events and is very useful to avoid spurious and/or uncorrelated contributions. In the middle and lower panels of fig.5b) are also shown two ToT spectra corresponding to the scattered  $^{17}\text{F}$  ions and to the light particles respectively. In the present case, we clearly see that the  $^{17}\text{F}$  scattering events have a ToT sharply peaked around 400 ns ( $6 \times 67$  ns), while for light particles the ToT is smaller than 266 ns ( $4 \times 67$  ns). The ToT is only roughly proportional to the energy released by the particles into the strip, but it is very useful to disentangle the hitting positions when two particles, with very different energy ranges, contemporarily impinge on the same detector.

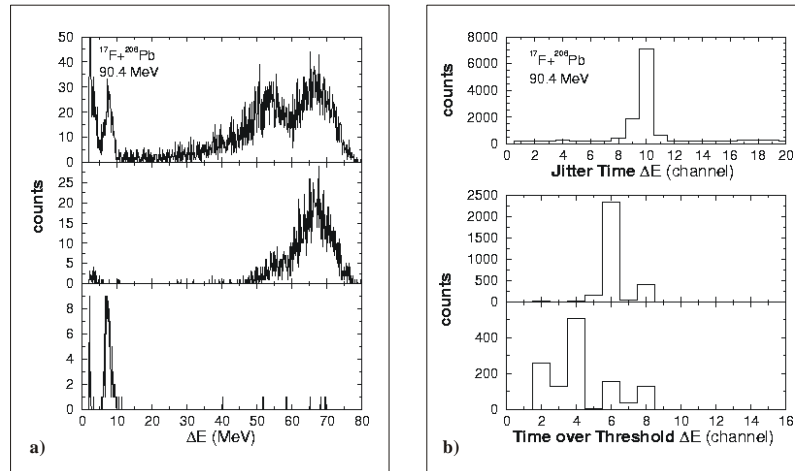


**FIGURE 5.** a)  $\Delta E$  spectrum collected from the backward detector of the EXODET apparatus. Total spectrum (upper panel), gated by JT=10 and ToT=6 (middle panel), gated by JT=10 and ToT ranging from 2 to 4 (lower panel). b) Jitter Time (JT) spectrum of the backward  $\Delta E$  detector (upper panel). Time over Threshold (ToT) spectra of the backward  $\Delta E$  detector collected with the following gates: JT=10 and  $\Delta E > 59$  MeV, corresponding to the  $^{17}\text{F}$  peak, (middle panel); JT=10 and  $\Delta E < 10$  MeV, corresponding to the light particles range, (lower panel).

The distribution over the strips of the scattered  $^{17}\text{F}$  ions was corrected for the strip geometrical efficiency, using Monte-Carlo calculations to evaluate the solid angles and the  $\theta_{\text{lab}}$  scattering angle ranges subtended by each strip, with an uncertainty estimated less than 1%. The normalization of the cross section was obtained considering the  $^{17}\text{F}$  scattering in the forward detector as a purely Rutherford one.

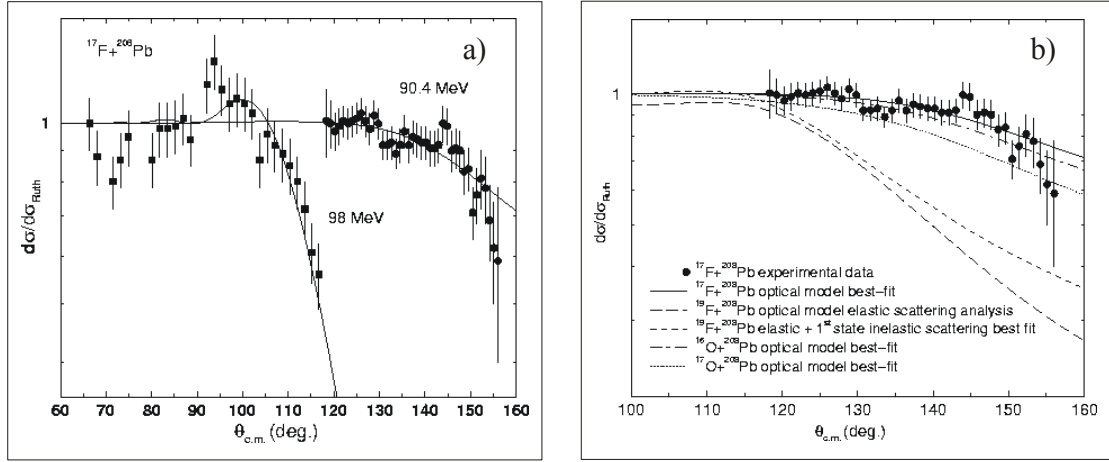


**FIGURE 6.** a) Angular distribution of the  $^{17}\text{F}$  at 90.4 MeV incident energy (present experiment) and at 98 MeV (ORNL experiment [2]). The solid lines represent optical model best fits. b) The data and the optical model best-fit for  $^{17}\text{F}$  are compared with those of other nuclei. The  $^{17}\text{F}$  behavior results more similar to those of the  $^{16}\text{O}$  and  $^{17}\text{O}$  than to the  $^{19}\text{F}$  one.

## RESULTS AND COMMENTS

In fig.6a) the angular distribution of the scattered  $^{17}\text{F}$  ions is presented. Because of the target thickness and of the target frame screening, only the experimental points above  $115^\circ$  could be evaluated. For comparison, the data for the same system at 98 MeV of beam energy have been also reported. This experiment [2] was performed at the Holifield Radioactive Ion Beam Facility, ORNL, Oak Ridge (USA), with a  $^{17}\text{F}$  beam produced through the direct reaction  $^{16}\text{O}(d, n)^{17}\text{F}$ . The continuous lines are optical model best fits obtained with the code SFRESCO [3], using the same parameter set ( $a_v=a_w=0.53$  fm,  $V_0=52.7\pm 6.2$  MeV,  $r_{0v}=r_{0w}=1.24$  fm) and leaving free only the depth of the imaginary potential ( $W_0=7.1\pm 1.8$  MeV and  $W_0=15.9\pm 2.9$  MeV for the 90.4 MeV and 98.0 MeV data, respectively). We could not experimentally distinguish the contribution of the inelastic scattering to the total scattering cross section, because it requires an energy resolution better than 0.7%. So we did not include in our calculations the excitation of the first excited state of  $^{17}\text{F}$  (at 0.4953 MeV). We checked *a posteriori* the validity of our assumption, running the code FRESCO [3] within the DWBA, using as potential parameters those obtained by the best fit and including the first excited state with the experimental transition probability  $B(E2)\uparrow=21.64$  e<sup>2</sup>fm<sup>4</sup> [4]. We found that the contribution of this channel to the quasi-elastic cross section is less than 2%, in the energy range here considered, and therefore it could be neglected in first approximation.

A comparison of the scattering angular distributions for four different systems is shown in fig.6b) [2,5,6]. In table 1 the optical model potential parameters obtained from the best-fit analyses are reported. The behavior of the  $^{17}\text{F}$  angular distribution results more similar to those of the Oxygen isotopes than to the  $^{19}\text{F}$  one, also if we consider the quasi-elastic contribution coming from the first excited state of the  $^{19}\text{F}$  (at 0.197 MeV). The difference between the  $^{17}\text{F}$  and  $^{19}\text{F}$  projectiles is evidenced also by

the reaction cross section that is three times larger for  $^{19}\text{F}$ . The explanation of such a different behavior could be found in the completely different structure of the two nuclei:  $^{17}\text{F}$  is a weakly bound radioactive nucleus, while  $^{19}\text{F}$  is well bound with a rotational band. The  $^{16}\text{O}$  and  $^{17}\text{O}$  nuclear structures are quite similar to that of  $^{17}\text{F}$  even if their binding energies are much higher.

**TABLE 1. Optical model potential best-fit parameter.**

reaction	$E_{\text{lab}}$ (MeV)	$E_{\text{cm}}/V_c$	$V_0$ (MeV)	$r_{0v}$ (fm)	$a_v$ (fm)	$W_0$ (MeV)	$r_{0w}$ (fm)	$a_w$ (fm)	$\chi^2/\text{pt}$	$\sigma_R$ (mb)
$^{17}\text{F}+^{208}\text{Pb}$	90.4	0.96	$52.7 \pm 6.2$	1.24	0.53	$7.1 \pm 1.8$	1.24	0.53	0.525	77
$^{19}\text{F}+^{208}\text{Pb}$	91	0.96	$107.6 \pm 6.1$	1.24	0.53	$20.1 \pm 3.0$	1.24	0.53	1.111	269
$^{16}\text{O}+^{208}\text{Pb}$	78	0.93	78.28	1.215	0.65	17.11	1.162	0.623	0.99	47
$^{17}\text{O}+^{208}\text{Pb}$	78	0.93	82.21	1.226	0.65	9.93	1.226	0.60	1.25	91

Despite the small beam time used to collect data (about 17 hours), we performed also a search for  $^{17}\text{F} \rightarrow \text{p}+^{16}\text{O}$  break-up events. We considered only the events in which: a) two strips of the  $\Delta E$  detector and only one of the E detector should be hit; b) the JT of all the strips should be in the correlation peak; c) the ToT of one strip of the  $\Delta E$  detector should be in the Fluorine-Oxygen range; d) the ToT of the other strip of the  $\Delta E$  detector should be lower; e) the total energy released in the  $\Delta E$  detector should be in the spectrum region of the  $^{17}\text{F}$ - $^{17}\text{O}$  peaks (corresponding to the total energy of the  $^{16}\text{O}$  plus the energy lost by the proton passing through the  $\Delta E$ ). A value  $\sigma_{\text{BU}}=(3.1 \pm 1.4)$  mb was obtained for the break-up cross section in good agreement with that extracted from literature [7] ( $\sigma_{\text{BU}}=1.6 - 3.2$  mb).

In summary, we reported about the features and the performances of the new experimental apparatus EXODET, designed to be used in RIB experiments. The use of an ASIC chip for the readout electronics allows high performances at a relatively low cost and the integration of energy and chip information gives the possibility of strong data selection. In the first experiment, successfully performed using the EXODET apparatus, the  $^{17}\text{F}+^{208}\text{Pb}$  scattering at 90.4 MeV has been studied. The  $^{17}\text{F}$  angular distribution has been measured and an optical model analysis performed to extract the best-fit potential parameter set. We have found that the  $^{17}\text{F}$  scattering behavior is consistent with the  $^{17}\text{F}$  data taken at higher energy. By the comparison with other systems, we have seen that such behavior is very different from that of the  $^{19}\text{F}$  one, in the same energy range, but it is quite similar to those of  $^{16}\text{O}$  and  $^{17}\text{O}$ .

## REFERENCES

1. Perazzo, A., et al., *BABAR Note #501* (1999) and references therein.
2. Lin, C. J., et al., *Phys. Rev. C* **63**, 064606 (2001).
3. Thompson, I. J., *Comput. Phys. Rep.* **2**, 167 (1998).
4. Tilley, D. R., et al., *Nucl. Phys. A* **565**, 1 (1993).
5. Thompson, I. J., et al., *Nucl. Phys. A* **505**, 84 (1989).
6. Lilley, J. S., et al., *Nucl. Phys. A* **463**, 710 (1987).
7. Rehm, K. E., et al., *Phys. Rev. Lett.* **81**, 3341 (1998).